A&A 631, A29 (2019)
https://doi.org/10.1051/0004-6361/201935618
© ESO 2019

Astronomy & Astrophysics

MCDHF and RCI calculations of energy levels, lifetimes, and transition rates in Si III and Si IV★

B. Atalay[1,2], T. Brage[1,4], P. Jönsson[3], and H. Hartman[3]

[1] Department of Physics, Lund University, Post Office Box 118, 22100 Lund, Sweden
e-mail: betul.atalay@teorfys.lu.se
[2] Department of Physics, Çanakkale Onsekiz Mart University, Çanakkale, Turkey
e-mail: batalay@comu.edu.tr
[3] Materials Science and Applied Mathematics, Malmö University, 20506 Malmö, Sweden
[4] Institute of Modern Physics, Fudan University, Shanghai, PR China

Received 4 April 2019 / Accepted 4 August 2019

ABSTRACT

We present extensive multiconfiguration Dirac-Hartree-Fock and relativistic configuration interaction calculations including 106 states in doubly ionized silicon (Si III) and 45 states in triply ionized silicon (Si IV), which are important for astrophysical determination of plasma properties in different objects. These calculations represents an important extension and improvement of earlier calculations especially for Si III. The calculations are in good agreement with available experiments for excitation energies, transition properties, and lifetimes. Important deviations from the NIST-database for a selection of perturbed Rydberg series are discussed in detail.

Key words. atomic data

1. Introduction

Silicon is one of the most abundant elements on Earth and in the Universe. Due to its high abundance, the lowest ionization ions of Silicon, Si I-IV, play important roles in the diagnostics and modeling of various astrophysical (Becker & Butler 1990; Catanzaro et al. 2008; Iijima & Nakanishi 2008) and laboratory plasmas (Cowpe et al. 2008; Yamazaki et al. 2009; Ogilvie & Nicolich 2009). Si I and Si II have been extensively studied both experimentally and theoretically, see for example Pehlivan Rhodin (2018) and references given therein.

Lines from Si III and Si IV are observed in the spectra of several different astronomical objects, for example the solar corona and transition region, early-type stars, planetary nebulae, novae, and the interstellar medium, where they have been used for diagnostics of the plasma parameters (Dufton et al. 1983; Nussbaumer 1986; Rubin et al. 1993). As an example, Dufton et al. (1983) used the Si III emission lines observed by Skylab to determine the electron density of the solar corona. Discrepancies between observed and predicted Si III line ratios involving the intercombination line $3s^2\ ^1S_0$–$3s3p\ ^3P_1$ at 1892 Å and the higher excitation $3s3p\ ^1P_1$–$3s4s\ ^1S_0$ at 1313 Å were found. The authors suggested it may have been caused by the presence of a non-Maxwellian electron distributions changing the intensity ratio between the lines. The energy of the upper level of the 1313 Å line is considerably higher than the average electron thermal energy, and the excitation from the ground state can be increased by high-energy electrons (Pinfield et al. 1999). Similarly, Keenan et al. (1989) presented Spacelab 2 observations and Pinfield et al. (1999) presented spectra from the Solar Ultraviolet Measurements of Emitted Radiation (SUMER) instrument on-board the Solar and Heliospheric Observatory (SOHO) to give a deeper analysis of possible non-Maxwellian emission-line enhancement in different solar regions. The suggestion of the presence of non-Maxwellian electron distributions was followed up by Dzifčáková & Kulinová (2011). More recently, Del Zanna et al. (2015) investigated the main spectral diagnostics for Si III ultraviolet lines, to measure electron densities and temperatures. However, they found no conclusive evidence for the presence of non-Maxwellian electron distributions from observations of the low transition region of the solar atmosphere, based on *R*-matrix scattering calculations for electron collisional excitation of Si III, carried out with the intermediate-coupling frame transformation method. The updated and more accurate atomic data of Si III in the present paper, can be used for rederivation of the plasma diagnostics using existing solar observations.

Due to their relatively high ionization energies, lines from Si III and Si IV appear in early-type stars, for example B-type stars, which are massive stars with surface temperatures 10 000–30 000 K showing strong Si III and Si IV lines in their optical spectra. The present-day chemical abundances of the Galaxy in the solar vicinity, can be determined by studying B-type main sequence stars due to their short lifetimes (Przybilla et al. 2008; Simón-Díaz 2010). The silicon ionization balance is used as the temperature diagnostics in the B-type star temperature range. Becker & Butler (1990) used Si III and Si IV spectral lines to determine the temperature, whereas Monteverde et al. (2000) studied the ionization equilibria of Si III compared to Si II and Si IV, respectively, to find the Si-abundance. A recent study by Nieva & Przybilla (2012) analyzed 29 early B-type stars in OB associations with a thorough and self-consistent analysis technique. They found the present-day Solar neighborhood to be

★ Tables 1 and 2 are only available at the CDS via anonymous ftp to cdsarc.u-strasbg.fr (130.79.128.5) or via http://cdsarc.u-strasbg.fr/viz-bin/cat/J/A+A/631/A29

chemically homogeneous, indicating abundance fluctuations of less than 10% around the mean. Bailey & Landstreet (2013) carried out a study on the determination of the abundance of Si to clarify discordant results in mid to late B-type stars.

The atomic data parameters, particularly transition rates, are essential in the abundance determination and plasma modeling. The work presented here therefore aims to provide accurate atomic data for a large part of the Si III and Si IV spectrum.

2. Previous work on atomic data for Si III and Si IV

Berry et al. (1971) and Livingston et al. (1976a,b) performed radiative lifetime measurements in Si III and Si IV using the beam-foil technique. Kwong et al. (1983) used a radio-frequency ion trap to measure the lifetime of the long-lived $3s3p\ ^3P^o_1$ level of Si III by observation of the decay to the ground state at 1892 Å and obtained an A-value of $(1.67 \pm 0.1) \times 10^4\ s^{-1}$. This result has been included in many later plasma models. Later studies, for instance Ojha et al. (1988), confirm this value.

On the theoretical side, Nussbaumer (1986) used a multiconfiguration approach with an adjustable Thomas–Fermi potential to determine the transition probabilities for the 17 lowest terms in Si III. They applied various semi-empirical corrections based on the observed energies to improve the accuracy in the term energies. Butler et al. (1993) computed the radiative data for the $3l3l'$ transitions, for Si III and other Mg-like ions of astrophysical interests by using the close-coupling approximation with a modified version of the R-Matrix code as a part of the international Opacity project (Seaton 1987). Safronova et al. (2000) used relativistic second-order many body perturbation theory (MBPT) to calculate excitation energies and transition rates for the same transition arrays. Almaraz et al. (2000) applied the CIV3 code (Hibbert 1975) to calculate energy levels and oscillator strengths in Si III.

In more recent studies, Del Zanna et al. (2015) performed a large-scale R-matrix scattering calculation providing 149 LS terms and 283 fine-structure levels arising from $3snl$, $3pnl$ and $3dnl$ configurations with $n \leq 5$ and $l \leq 4$. Aggarwal (2017) reported energies and lifetimes for the 141 levels of the $3l3l'$ and $3l4l'$ configurations and radiative rates for four types of transitions (E1, E2, M1, and M2) in Si III. Iorga & Stancalie (2018) investigated the effect of core-valence and core-core correlations on the energy levels and transition probabilities in the Mg isoelectronic sequence using the Flexible Atomic Code (FAC; Gu 2008). The results contained the energy of the levels arising from the valence configurations along with transition rates corresponding to E1, M1, E2, M2 transitions between states arising from $3l3l'$ with $l, l' \leq 2$ and $3snl''$ with $n \leq 7$ and $l'' \leq 4$ configurations.

Froese Fischer et al. (2006) performed extensive and highly accurate multiconfiguration Hartree-Fock (MCHF) calculations for the Mg-like sequences ($Z = 12, \ldots, 26$). They used Breit-Pauli approximation to include relativistic effects. They computed both allowed (E1) and some forbidden (E2, M1, M2) transitions.

For triply ionized silicon Maniak et al. (1993) performed radiative lifetime measurements of 3p, 3d, and 4s levels using the beam-foil technique. Theodosiou & Curtis (1988) used a semi-empirical quantum defect approach to calculate lifetimes for the $3p\ ^2P_{1/2}$, $3p\ ^2P_{3/2}$, $3d\ ^2D_{3/2}$, and $3d\ ^2D_{5/2}$ levels in the Na isoelectronic sequence. These calculations reached a fair agreement with experiments, but deviated from some ab initio results. Siegel et al. (1998) used a semi-empirical model potential approach to compute electric dipole transition oscillator strengths for low-lying transitions in the Na isoelectronic sequence (Na I–Ca X). The core polarization effects were explicitly included in the calculations. Siems et al. (2001) presented oscillator strengths and lifetimes for Si IV using a multiconfiguration Hartree-Fock relativistic (HFR) approach. In recent years, Nandy & Sahoo (2015) carried out calculations of the relativistic sensitivity coefficients, oscillator strengths, transition probabilities, lifetimes, and magnetic dipole hyperfine structure constants for a number of low-lying states in the Zn II, Si IV, and Ti IV. Safronova et al. (1998) carried out all-order relativistic many-body calculations of removal energies and hyperfine constants for 3s, $3p_{1/2}$, $3p_{3/2}$, $3d_{3/2}$,$3d_{5/2}$, and 4s states of Na-like ions with $Z = 11-16$. The reduced dipole matrix elements were determined for $3p_{1/2}-3s$, $3p_{3/2}-3s$, $4s-3p_{1/2}$, $4s-3p_{3/2}$, $3d_{3/2}-3p_{1/2}$, $3d_{3/2}-3p_{3/2}$, and $3d_{5/2}-3p_{3/2}$ electric-dipole transitions. The calculations included single and double excitations of the Hartree–Fock ground state to all orders in perturbation theory. Theoretical fine-structure intervals had an agreement with measurements to about 0.3% for 3p states and to about 3% for 3d states. Theoretical hyperfine constants and line strengths agreed with the precise measurements to better than 0.3%. Finally, Froese Fischer et al. (2006) performed extensive ab initio non-orthogonal spline CI calculations for the Na-like sequence. Kelleher & Podobedova (2008) presented the latest compilation of Si III and Si IV transition rates.

3. Theory

In this work, the calculations were performed using the fully relativistic multi-configuration Dirac-Hartree-Fock (MCDHF) method in jj-coupling (Grant 2007; Froese Fischer et al. 2016).

3.1. Multiconfiguration Dirac-Hartree-Fock

An electronic state of a many electrons system is determined by a wave function Ψ, which is a solution to the wave equation:

$$H\Psi = E\Psi, \tag{1}$$

where H is the Hamiltonian operator and E is the total energy of the system. The common starting point of the MCDHF method is the Dirac-Coulomb Hamiltonian:

$$H_{\rm DC} = \sum_{i=1}^{N} \left(c\boldsymbol{\alpha}_i \cdot \boldsymbol{p}_i + (\beta_i - 1)c^2 + V_{\rm nuc}(r_i) \right) + \sum_{i>j}^{N} \frac{1}{r_{ij}}, \tag{2}$$

where $V_{\rm nuc}(r_i)$ is the monopole part of the electron-nucleus Coulomb interaction, r_{ij} is the distance between electrons i and j, $\boldsymbol{\alpha}$ and β are the 4-by-4 Dirac matrices, and c is the speed of light.

The approximate solutions to the wave equations are referred to as atomic state functions (ASFs). An atomic state function, $\Psi(\gamma PJ)$, is in our approach represented by a linear combination of configuration state functions (CSFs),

$$\Psi(\gamma PJ) = \sum_{j=1}^{N_{\rm CSFs}} c_j \Phi(\gamma_j PJ), \tag{3}$$

where P is the parity and J is the total angular momentum. γ_j represents all necessary quantum numbers and the orbital occupancy to define the CSF, while c_j are the mixing coefficients. The γ is usually selected as the γ_j corresponding to the largest weight $|c_j|^2$.

The CSFs are in turn constructed as angular-momentum-coupled, anti-symmetrized products of one-electron Dirac-orbitals of the form

$$\psi(r) = \psi_{n\kappa,m}(r) = \frac{1}{r}\begin{pmatrix} P_{n\kappa}(r)\chi_{\kappa,m}(\theta,\varphi) \\ \mathrm{i}Q_{n\kappa}(r)\chi_{-\kappa,m}(\theta,\varphi) \end{pmatrix}, \quad (4)$$

where $P_{n\kappa}(r)$ and $Q_{n\kappa}(r)$ are the large and small components of the radial wave function, and $\chi_{\pm\kappa,m}(\theta,\varphi)$ are two-component spin-orbit functions.

The extended optimal level (EOL) scheme is used to determine energies and wave functions. In the EOL scheme, the radial parts of the Dirac orbitals and the expansion coefficients of the targeted states are optimized to self-consistency by solving the MCDHF equations, which are derived using the variational approach (Dyall et al. 1989). In subsequent relativistic configuration interaction (RCI) calculations the transverse photon interaction (Breit interaction)

$$H_{\mathrm{Breit}} = -\sum_{i<j}^{N}\left[\boldsymbol{\alpha}_i\cdot\boldsymbol{\alpha}_j\frac{\cos(w_{ij}r_{ij}/c)}{r_{ij}} + (\boldsymbol{\alpha}_i\cdot\boldsymbol{\nabla}_i)\left(\boldsymbol{\alpha}_i\cdot\boldsymbol{\nabla}_j\right)\frac{\cos(w_{ij}r_{ij}/c)-1}{w_{ij}^2 r_{ij}/c^2}\right] \quad (5)$$

may be included in the Hamiltonian (McKenzie et al. 1980). The photon frequency w_{ij}, used by the RCI program in calculating the matrix elements of the transverse photon interaction, is taken as the difference of the diagonal Lagrange multipliers associated with the orbitals. The leading quantum electrodynamic (QED) corrections effects, in the form of self-energy and vacuum polarization, are also included. The CSFs are given in the jj-coupling scheme during this procedure, but to make a comparison with experiments more feasible, we transform the resulting wave function to the LSJ-coupling scheme, using the JJ2LSJ program (Gaigalas et al. 2003, 2004, 2017) part of the GRASP2K code (Jönsson et al. 2013). All the calculations were performed with an updated parallel version of the GRASP2K code by Jönsson et al. (2013). To calculate the spin-angular part of the matrix elements, the second quantization method in coupled tensorial form and quasispin technique (Gaigalas et al. 1997, 2001) were adopted.

3.2. Computation of transition parameters

Once well-converged and effectively complete ASFs have been obtained radiative transition such as transition probabilities and weighted oscillator strengths can be determined. The transition parameters between two states γJM and $\gamma' J' M'$ are expressed in terms reduced matrix elements

$$\langle\Psi(\gamma PJ)\|\mathbf{T}\|\Psi(\gamma' P' J')\rangle = \sum_{j,k} c_j c'_k \langle\Phi(\gamma_j PJ)\|\mathbf{T}\|\Phi(\gamma'_k P' J')\rangle, \quad (6)$$

where $\mathbf{T}$ is the transition operator (Grant 1974).

For electric multipole transitions, there are two forms of the transition operator, the length (Babushkin gauge) and velocity (Coulomb gauge) forms (Grant 1974). Due to the definition of these two, the length form is more sensitive to the outer part of the wave functions, which are usually active in radiative transitions. A number of studies have shown that the length form generally gives more reliable values at a given level of valence and core-valence electron correlation although the velocity form seems to be more stable for transitions including highly excited Rydberg states (Pehlivan Rhodin et al. 2017). It is common to use the agreement between transition rates A_l and A_v computed in two forms as an indicator of accuracy of the wave functions (see review by Froese Fischer 2009; Ekman et al. 2014). A possible measure of this is the quantity $\mathrm{d}T$, characterizing the uncertainty of the calculated transition rates and defined as

$$\mathrm{d}T = \frac{|A_l - A_v|}{\max(A_l, A_v)}, \quad (7)$$

where A_l and A_v are the transition rates in length and velocity forms respectively. The values of $\mathrm{d}T$ do not represent uncertainty estimates for each individual transition but should be considered as statistical indicators of uncertainties within given sets of transitions.

4. Calculations

Our MCDHF and RCI calculations for doubly and triply ionized silicon started by defining a multireference (MR) set of configurations. From this we allow single and double substitutions to a systematically increasing active set of orbitals.

4.1. Si III

In doubly ionized silicon, calculations were performed for states belonging to the $3s^2$, the $3p^2$; the 3p4p; the 3sns with $n = 4,\ldots,9$; the 3snd with $n = 3,\ldots,8$; the 3sng with $n = 5,\ldots,8$ even configurations and furthermore, the 3snp with $n = 3,\ldots,9$; the 3snf with $n = 4,\ldots,8$; the 3pnd with $n = 3, 4$; and the 3p4s odd configurations. These configurations define the MR for the even and odd parities, respectively. Terms involving configurations with $n = 8$ and 9 do not belong to our targeted states but they are taken into account to obtain orbitals with large radii to get a reasonable agreement between length and velocity form for the transition properties, see Pehlivan Rhodin et al. (2017).

In the first step of our calculations, an initial MCDHF calculation in the EOL scheme (Dyall et al. 1989) was performed simultaneously for all even and odd multireference states. These initial calculations were followed by calculations with expansions including the configuration state functions (CSFs) obtained by single (S), double (D) substitutions of electrons from the spectroscopic reference configurations to the active set of orbitals (Olsen et al. 1988; Sturesson et al. 2007).

In an restricted active set approach (RAS) restrictions are put on the allowed substitutions from the MR, when generating the full space of CSFs. We therefore define the valence region of the atom as the two outer electrons, outside the $1s^2 2s^2 2p^6$ core subshells. We kept the $1s^2$-subshell fixed in all calculations, that is, not allowing substitutions from it. After optimizing simultaneously the even and odd states of the MR-set in the first step of calculations, our goal was to include valence-valence (VV) and core-valence (CV) interaction to convergence. We optimized four layers of correlation orbitals based on the VV correlation, only allowing SD substitutions from the valence subshells. The orbitals in the active set were systematically extended to include orbitals up to the 13s,13p,12d,12f,12g, and 9h in the final correlation layer. These MCDHF calculations were followed by RCI calculations including Breit-interaction and some QED effects as described above.

As a final step of our work, an RCI calculation was performed. The expansion for that RCI calculation was obtained by augmenting the largest SD valence expansion with a CV expansion. The CV expansion was generated by SD substitutions

from the valence orbitals and the $2p^6$ core with the restriction that there should be at the most one substitution from the 2s or 2p subshells. We neglected core-core (CC) correlation, meaning more than one excitation from the core, which was comparatively unimportant for both the energy separations and the transition probabilities (Zou & Fischer 2000). The resulting expansions consisted of 1 401 150 and 1 760 209 CSFs distributed over the $J = 0, 1, \ldots, 6$ symmetries for even and odd parity, respectively.

4.2. Si IV

In triply ionized silicon, calculations were performed for states belonging to the configurations $2s^22p^6nl$ where $n \leq 9$ and $l \leq 6$, defining the MR configurations. We again added two more layers of spectroscopic orbitals, $n = 8, 9$, in comparison with the states we were targeting to get a reasonable agreement between length and velocity form for the transition properties.

As a starting point for the calculations, MCDHF calculations in the EOL scheme were performed for the even and odd parity states in the MR simultaneously. The initial calculations were followed by separate calculations in the EOL scheme for the even and odd parity states, where the CSFs were obtained by allowing SD substitutions from the configurations in the MR to active orbital sets, which were consecutively enlarged by layers of correlation orbitals. Si IV has one electron outside closed subshells, and consequently there is no VV correlation. The corrections to our results can therefore be classified as CV and CC correlations. The major effect comes from the CV correlation. The CV expansion was obtained by restricting the substitutions in such a way that only one substitution was allowed from the 2s or 2p subshells of the configurations in the MR, and no substitutions from the 1s shell, this means that 1s shell was an inactive closed core.

The active sets of orbitals for the even and odd parity states were extended by layers to include orbitals with quantum numbers $n \leq 12$ and $l \leq 6$. Each MCDHF calculation was followed by RCI calculations, including the Breit-interaction and leading QED effects. We investigated the CC correlation effects by optimizing one layer of orbitals $n = 13$ on SD from the $2s^22p^6$ core in an RCI calculation as a final step of our work. The number of CSFs in the final even and odd state expansions were approximately 995 020 and 993 501, respectively, distributed over the different J symmetries.

5. Results

5.1. Si III

We present in Table A.1 the computed excitation energies in Si III for increasing active sets of orbitals labeled with the highest principal quantum number n of the orbitals in the active set. The calculations including only VV correlation, built on three layers of correlation orbitals, is followed by finally including the CV correlation using an RCI-approach.

The computed excitation energies are in good agreement with the values from the NIST-database (Kramida et al. 2018). For the VV correlation, the mean relative difference between theory and experiment is of the order of 0.9%. The inclusion of CV correlation effects improves the energies dramatically since the values for all computed energy separations have converged.

The final excitation energies are in good agreement with the experimental ones, with a mean difference of only 0.05%. For comparison, the experimental energies from the NIST Atomic Spectra Database (Kramida et al. 2018) and also the differences ΔE, between the observed energies and the final computed excitation energies, are given in Table A.1.

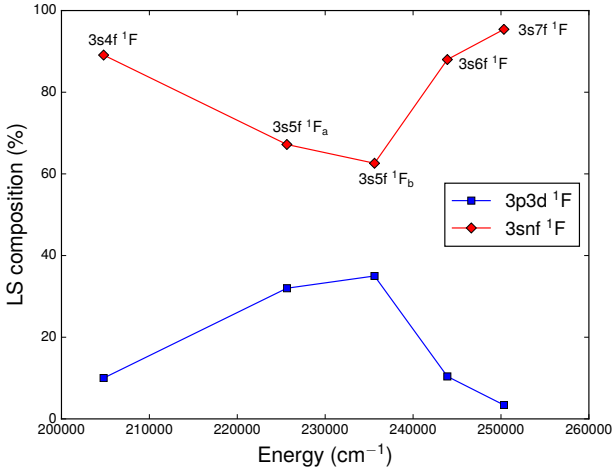

Fig. 1. 3p3d and 3snf composition of $^1F^o$ Rydberg series members.

There is excellent agreement between observations and calculations for most of the levels, with a few important exceptions, due to mislabeling of levels. The NIST label classification for Si III is based on the analysis done by Toresson (1961). Since then the NIST designations for the 3p3d ^{1}P and the 3p4s ^{1}P have been interchanged as recommended by Victor et al. (1976) and Zetterberg & Magnusson (1977). The assignments for 3p3d ^{1}P and 3p3d ^{1}F levels have been questioned previously by Reistad et al. (1984) and Brage & Hibbert (1989).

If we start by investigating the $^1F^o$-levels, we note that the 3p3d $^1F^o$ perturbs the 3snf Rydberg series. This perturbation has been studied by a number of authors along the Mg-sequence (Brage & Hibbert 1989; Reistad et al. 1984; Aashamar et al. 1986). The NIST classification identifies the level at 235 413 cm^{-1} as 3p3d ^{1}F for convenience, even though the calculated composition is 65% 3snf (Froese Fischer & Godefroid 1982). To illustrate the complexity of the situation, we show the composition of the ^{1}F levels in Fig. 1. It is clear that the 3p3d ^{1}F is not the major component for any state and that the same CSF 3s5f $^1F^o$ is the largest component for two levels. We therefore choose to change the designation as shown in Table A.1 where these two levels are labeled as 3s5f $^1F^o_{3\,a}$ and 3s5f $^1F^o_{3\,b}$, respectively.

Our second example of a strongly perturbed series investigated by Froese Fischer & Godefroid (1982) is a short-range interaction of the plunging configuration 3p3d ^{1}P with the 3snp ^{1}P Rydberg series. In Si III the 3s6p $^1P_1$ and 3p3d $^1P_1$ are close to degenerate and the labeling of these levels is hard to reproduce. A closer look at the LS-percentage composition and excitation energies of 3snp ^{1}P and 3p3d ^{1}P are shown in Fig. 2, where the level at 234 923 cm^{-1} is best represented as 3p3d ^{1}P. Also in this case we adjust the labels from NIST.

A third example of a complicated case of level-designation is the 3snd $^1D^e$ Rydberg series, which is perturbed by the $3p^2$ ^{1}D for low excitations and the 3p4p $^1D_2$ for $n = 6$–8. In our calculations the level energy of 3s7d $^1D_2$ is 247 946 cm^{-1}, while the values given by NIST is 250 636 cm^{-1}. However, the LS composition of the former level is 72% 3s7d $^1D_2$ and 18% 3p4p $^1D_2$. We suggest that the NIST identification of the level $^1D_2$ at 250 636 cm^{-1} and at 247 935 cm^{-1} should be interchanged as shown in Table A.1.

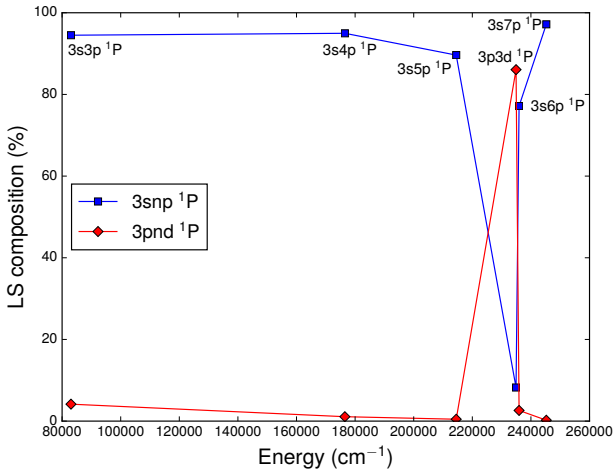

Fig. 2. 3pnd ^{1}P and 3snp composition of ^{1}P^o Rydberg series members.

A problem in spectroscopic calculations, that includes a large number of states, is to reproduce very close degeneracy between some levels. An example of this is the relative position of the singlet and triplet levels the 3snp Rydberg series with $n = 6–7$. It is clear that we are not able to reproduce the NIST-values for the relative position of these levels, which makes, for example, our values for intercombination lines inaccurate from the 3s6p and 3s7p ^{3}P-levels.

In Table A.2, the current results for the 29 lowest excitation energies of Si III are compared with the ones from the MCHF-BP calculations by Froese Fischer et al. (2006) and *R*-matrix calculations by Del Zanna et al. (2015). To make the comparison easier the differences between observed and computed energies are also given in the last columns for the different computational approaches. From the comparison, it is clear that the agreement with the present RCI calculations and the MCHF-BP calculations is very good. Furthermore, the agreement between the current RCI results and the observed energies is improved especially above the 3p^2 ^{1}S$_0$ level.

The complete transition data table, using the length form of transition operator, including rates, weighted oscillator strengths, wavenumber, and the uncertainty in the computed rates, for E1 transitions in Si III for the wavelength range of 40–18 239 nm is available at the CDS. The wavenumber and wavelength values are changed to match the values in the NIST database, which are the values from Reader et al. (1980). Uncertainties of the transition rates have been estimated from the expressions suggested by Ekman et al. (2014). The estimated relative uncertainties for most of the strong transitions are below 1%. For many weak transitions the uncertainties are around 10%. However, for weak intercombination transitions the uncertainties are considerably large due to difficulties in calculating the transition rates of intercombination lines. There are some weak two-electron one-photon transitions with large uncertainties. These transitions are zero in the single configuration approximation and are allowed only through correlation effects. Thus, the two-electron one-photon transitions are very difficult to compute and the uncertainties are often large.

The 3s4s ^{1}S$_0$ $\rightarrow$ 3s3p ^{1}P$_1$ transition is of special importance in the diagnostics of non-Maxwellian electron distributions, as discussed above. According to Dufton et al. (1983) the rate for this transition is 2.8×10^8 s^{-1}, while Nussbaumer (1986) predicted 4.0×10^8 s^{-1} and Del Zanna et al. (2015) 2.96×10^8 s^{-1}. Our result for this rate is 8.53×10^8 s^{-1} close to Froese Fischer et al. (2006) calculation of 8.99×10^8 s^{-1}.

Our estimated lifetimes (including only E1-transitions) for excited states of Si III are given in Table A.3. We also compare our results to available measurements in this table. Berry et al. (1971), Livingston et al. (1976b) and Bashkin et al. (1980) measured the lifetimes for a few levels in Si III with the beam foil method. The agreement between the current RCI results and measurements is quite satisfactory, though the results from the measurements of Berry et al. (1971) slightly differ from the RCI values. This may be explained by the uncertainties in the beam-foil method discussed by Zou et al. (1999). The lifetimes from the current RCI calculations are also compared to results from the MCHF-BP calculations by Froese Fischer et al. (2006) and MBPT calculations by Safronova et al. (2000), when these include all important transitions from a given state. The overall agreement is good, giving us confidence in the present results. For most states there is no major discrepancy between the current results and MBPT results except for the 3p3d ^{3}F$^o_{2,3,4}$ states. The reason for that is unclear, but for the rest of the states the discrepancies are quite small.

5.2. Si IV

In Table A.4, we present the level energies of the lowest 45 levels in Si IV as functions of increasing active sets of orbitals (labeled by the highest principal quantum number n). The calculations are based on CV correlation, including three layers of correlation orbitals. From the inspection of Table A.4, it is clear that the present calculations are well converged with respect to the increasing orbital set. The inclusion of CC correlation effects, adding one more layer of correlation orbitals with $n = 13$, improves the energies and the final energies are in good agreement with experiment displaying a mean difference of 0.09%. We present the experimental level energies from the NIST-database for Si IV in Table A.4, including the differences between the observed and the computed energies. In Table A.4, we also compare the present computed excitation energies with those from the non-orthogonal B-spline CI method (Zatsarinny & Fischer 2002) by Froese Fischer et al. (2006) for Si IV, showing excellent agreement.

The complete transition data table, using the length form of transition operator, including rates, weighted oscillator strengths, wavenumber, and the uncertainty in the computed rates, for E1 transitions in Si IV for the wavelength range of 31–11 933 nm can be found at the CDS. Uncertainties of the transition rates have been estimated from the expressions suggested by Ekman et al. (2014). The wavelength and wavenumber values are changed to match the values in the NIST database, which are the values from Reader et al. (1980). In general, the estimated relative uncertainties for most of the transitions are less than 10%. However, for some transitions the uncertainties are very large mostly due to difficulties in calculating the transition rates of intercombination lines and two-electron transitions.

Table A.5 presents our estimated lifetimes of the excited states (including only E1-transitions) in both length and velocity forms. The average relative difference between lifetimes in two forms is ~0.8%, which is highly satisfactory. This difference might be considered to be an internal validation of the accuracy of the calculations. The comparison of our results with previously reported theoretical and experimental values are also given in Table A.5. Siems et al. (2001) performed a HFR approach to estimate the lifetimes for Si IV. In that approach, the electrostatic parameters were optimized using a least-squares procedure. Berry et al. (1971) and later Bashkin et al. (1980) measured lifetimes using the beam-foil method. The overall

agreement between these measured lifetimes and the current lifetimes is rather good. From the table, one can see that our results are in excellent agreement with the results of Froese Fischer et al. (2006) and Siems et al. (2001).

6. Conclusions

In this work, we performed self-consistent MCDHF and subsequent RCI calculations for Si III and Si IV, as an extension and update to earlier calculations. Previous theoretical and experimental data were used to validate our results. Excitation energies from the RCI calculations are in a very good agreement with available observations. Our present study is an extension to the most accurate MCHF-BP and the BSR_CI calculations, and in general in excellent agreements with them. The presented results significantly increase the amount of accurate energy data of astrophysical interest for the two Si-ions. The highly accurate atomic data helps to correct interpretation of the lines. Therefore, we recommend our present results based on a fully relativistic method for abundance analysis and plasma diagnostics.

Acknowledgements. Betül Atalay acknowledges financial support from the Scientific and Technological Research Council of Turkey (TUBITAK) – BIDEB 2219 International Post-Doctoral Research Fellowship Program. Tomas Brage, Per Jönsson, and Henrik Hartman acknowledge support from the Swedish Research Council (VR) under contract No. 2015-04842. Dr Atalay also would like to express her appreciation of the hospitality shown by the Division of Mathematical Physics at Lund University and by the Department of Materials Science and Applied Mathematics at Malmö University.

References

Aashamar, K., Luke, T. M., & Talman, J. D. 1986, Phys. Scr., 34, 386
Aggarwal, K. M. 2017, At. Data Nucl. Data Tables, 117, 320
Almaraz, M. A., Hibbert, A., Lavín, C., Martín, I., & Bell, K. L. 2000, J. Phys. B: At. Mol. Opt. Phys., 33, 3277
Bailey, J. D., & Landstreet, J. D. 2013, A&A, 551, A30
Bashkin, S., Astner, G., Mannervik, S., et al. 1980, Phys. Scr., 21, 820
Becker, S. R., & Butler, K. 1990, A&A, 235, 326
Berry, H. G., Bromander, J., Curtis, L. J., & Buchta, R. 1971, Phys. Scr., 3, 125
Brage, T., & Hibbert, A. 1989, J. Phys. B: At. Mol. Opt. Phys., 22, 713
Butler, K., Mendoza, C., & Zeippen, C. J. 1993, J. Phys. B: At. Mol. Opt. Phys., 26, 4409
Catanzaro, G., Leone, F., Busá, I., & Romano, P. 2008, New Astron., 13, 113
Cowpe, J., Astin, J., Pilkington, R., & Hill, A. 2008, Spectrochim. Acta Part B: At. Spectr., 63, 1066
Del Zanna, G., Fernández-Menchero, L., & Badnell, N. R. 2015, A&A, 574, A99
Dufton, P. L., Hibbert, A., Kingston, A. E., & Doschek, G. A. 1983, ApJ, 274, 420
Dyall, K. G., Grant, I. P., Johnson, C. T., Parpia, F. A., & Plummer, E. P. 1989, Comput. Phys. Commun., 55, 425
Dzifčáková, E., & Kulinová, A. 2011, A&A, 531, A122
Ekman, J., Godefroid, M., & Hartman, H. 2014, Atoms, 2, 215
Froese Fischer, C. 2009, Phys. Scr. T, 134, 014019
Froese Fischer, C., & Godefroid, M. 1982, Phys. Scr., 25, 394
Froese Fischer, C., Tachiev, G., & Irimia, A. 2006, At. Data Nucl. Data Tables, 92, 607
Froese Fischer, C., Godefroid, M., Brage, T., Jönsson, P., & Gaigalas, G. 2016, J. Phys. B: At. Mol. Opt. Phys., 49, 182004
Gaigalas, G., Rudzikas, Z., & Froese Fischer, C. 1997, J. Phys. B: At. Mol. Phys., 30, 3747
Gaigalas, G., Fritzsche, S., & Grant, I. P. 2001, Comput. Phys. Commun., 139, 263
Gaigalas, G., Žalandauskas, T., & Rudzikas, Z. 2003, At. Data Nucl. Data Tables, 84, 99
Gaigalas, G., Zalandauskas, T., & Fritzsche, S. 2004, Comput. Phys. Commun., 157, 239
Gaigalas, G., Fischer, C., Rynkun, P., & Jönsson, P. 2017, Atoms, 5, 6
Grant, I. P. 1974, J. Phys. B: At. Mol. Opt. Phys., 7, 1458
Grant, I. 2007, in Relativistic Quantum Theory of Atoms and Molecules: Theory and Computation (Berlin: Springer), Springer Series on Atomic, Optical, and Plasma Physics
Gu, M. F. 2008, Can. J. Phys., 86, 675
Hibbert, A. 1975, Comput. Phys. Commun., 9, 141
Iijima, T., & Nakanishi, H. 2008, A&A, 482, 865
Iorga, C., & Stancalie, V. 2018, At. Data Nucl. Data Tables, 123, 313
Jönsson, P., Gaigalas, G., Bieroń, J., Fischer, C. F., & Grant, I. P. 2013, Comput. Phys. Commun., 184, 2197
Keenan, F. P., Cook, J. W., Dufton, P. L., & Kingston, A. E. 1989, ApJ, 340, 1135
Kelleher, D. E., & Podobedova, L. I. 2008, J. Phys. Chem. Ref. Data, 37, 1285
Kramida, A., Ralchenko, Yu, Reader, J., & NIST ASD Team 2018, NIST Atomic Spectra Database (ver. 5.5.6), [Online], Available: https://physics.nist.gov/asd [2018, April 16], National Institute of Standards and Technology, Gaithersburg, MD
Kwong, H. S., Johnson, B. C., Smith, P. L., & Parkinson, W. H. 1983, Phys. Rev. A, 27, 3040
Livingston, A. E., Baudinet-Robinet, Y., Garnir, H. P., & Dumont, P. D. 1976a, J. Opt. Soc. Am., 66, 1393
Livingston, A. E., Kernahan, J. A., Irwin, D. J. G., & Pinnington, E. H. 1976b, J. Phys. B: At. Mol. Opt. Phys., 9, 389
Maniak, S., Träbert, E., & Curtis, L. 1993, Phys. Lett. A, 173, 407
McKenzie, B. J., Grant, I. P., & Norrington, P. H. 1980, Comput. Phys. Commun., 21, 233
Monteverde, M. I., Herrero, A., & Lennon, D. J. 2000, ApJ, 545, 813
Nandy, D. K., & Sahoo, B. K. 2015, MNRAS, 447, 3812
Nieva, M. F., & Przybilla, N. 2012, A&A, 539, A143
Nussbaumer, H. 1986, A&A, 155, 205
Ogilvie, R. E., & Nicolich, J. 2009, Spectrochim. Acta Part B: At. Spectr., 64, 788
Ojha, P. C., Keenan, F. P., & Hibbert, A. 1988, J. Phys. B At. Mol. Phys., 21, L395
Olsen, J., Roos, B. O., Jørgensen, P., & Jensen, H. J. A. 1988, J. Chem. Phys., 89, 2185
Pehlivan Rhodin, A. 2018, PhD Thesis, Lund University
Pehlivan Rhodin, A., Hartman, H., Nilsson, H., & Jönsson, P. 2017, A&A, 598, A102
Pinfield, D. J., Keenan, F. P., Mathioudakis, M., et al. 1999, ApJ, 527, 1000
Przybilla, N., Nieva, M.-F., & Butler, K. 2008, ApJ, 688, L103
Reader, J., Corliss, C. H., Wiese, W. L., & Martin, G. A. 1980, Wavelengths and Transition Probabilities for Atoms and Atomic Ions: Part 1. Wavelengths, Part 2, Transition Probabilities (U.S. Government Printing Office)
Reistad, N., Brage, T., Ekberg, J. O., & Engström, L. 1984, Phys. Scr., 30, 249
Rubin, R. H., Dufour, R. J., & Walter, D. K. 1993, ApJ, 413, 242
Safronova, M. S., Derevianko, A., & Johnson, W. R. 1998, Phys. Rev. A, 58, 1016
Safronova, U. I., Johnson, W. R., & Berry, H. G. 2000, Phys. Rev. A, 61, 052503
Seaton, M. J. 1987, J. Phys. B: At. Mol. Phys., 20, 6363
Siegel, W., Migdalek, J., & Kim, Y.-K. 1998, At. Data Nucl. Data Tables, 68, 303
Siems, A., Luna, F., & Trigueiros, A. 2001, J. Quant. Spectr. Radiat. Transf., 68, 635
Simón-Díaz, S. 2010, A&A, 510, A22
Sturesson, L., Jönsson, P., & Froese Fischer, C. 2007, Comput. Phys. Commun., 177, 539
Theodosiou, C. E., & Curtis, L. J. 1988, Phys. Rev. A, 38, 4435
Toresson, Y. G. 1961, Ark. Fys. (Stockholm), 18, 389
Victor, G. A., Stewart, R. F., & Laughlin, C. 1976, ApJS, 31, 237
Yamazaki, H., Yoshiki, M., Takemura, M., Tomita, M., & Takeno, S. 2009, Spectrochim. Acta Part B: At. Spectr., 64, 808
Zatsarinny, O., & Fischer, C. F. 2002, J. Phys. B: At. Mol. Opt. Phys., 35, 4669
Zetterberg, P. O., & Magnusson, C. E. 1977, Phys. Scr., 15, 189
Zou, Y., & Fischer, C. F. 2000, Phys. Rev. A, 62, 062505
Zou, Y., Hutton, R., Huldt, S., et al. 1999, Phys. Scr. T, 80, 460

Appendix A: Additional tables

Table A.1. Computed excitation energies in cm^{-1} for Si III from different computational models.

Level	VV				CV	E_{obs} [a]	ΔE
	$n = 10$	$n = 11$	$n = 12$	$n = 13$			
$3s^2\ ^1S_0$	0	0	0	0	0	0	0
$3s3p\ ^3P^o_0$	51 539	51 541	51 561	51 604	52 790	52 725	−65
$3s3p\ ^3P^o_1$	51 656	51 671	51 686	51 728	52 913	52 853	−60
$3s3p\ ^3P^o_2$	51 893	51 938	51 941	51 981	53 164	53 115	−49
$3s3p\ ^1P^o_1$	83 380	83 186	83 145	83 094	83 031	82 884	−147
$3p^2\ ^1D_2$	120 291	120 305	120 314	120 361	122 447	122 215	−232
$3p^2\ ^3P_0$	128 668	128 658	128 667	128 703	129 832	129 708	−124
$3p^2\ ^3P_1$	128 808	128 794	128 796	128 832	129 953	129 842	−111
$3p^2\ ^3P_2$	129 043	129 052	129 046	129 080	130 193	130 101	−92
$3s3d\ ^3D_3$	141 773	141 743	141 761	141 794	143 106	142 944	−162
$3s3d\ ^3D_2$	142 183	141 743	141 762	141 805	143 162	142 946	−216
$3s3d\ ^3D_1$	142 470	141 743	141 762	141 812	143 208	142 948	−260
$3s4s\ ^3S_1$	151 757	151 808	151 821	151 875	153 332	153 377	45
$3p^2\ ^1S_0$	153 325	152 950	152 897	152 824	153 953	153 444	−509
$3s4s\ ^1S_0$	157 694	157 704	157 698	157 701	159 065	159 070	5
$3s3d\ ^1D_2$	166 150	165 215	165 198	165 172	166 013	165 765	−248
$3s4p\ ^3P^o_0$	173 433	173 475	173 497	173 551	175 219	175 230	11
$3s4p\ ^3P^o_1$	173 464	173 511	173 530	173 582	175 247	175 263	16
$3s4p\ ^3P^o_2$	173 533	173 589	173 601	173 648	175 312	175 336	24
$3s4p\ ^1P^o_1$	174 860	174 906	174 918	174 952	176 503	176 487	−16
$3p3d\ ^3F^o_2$	196 943	196 419	196 441	196 496	199 259	198 923	−336
$3p3d\ ^3F^o_3$	196 787	196 519	196 539	196 589	199 318	199 026	−292
$3p3d\ ^3F^o_4$	196 622	196 651	196 670	196 713	199 402	199 164	−238
$3s4d\ ^3D_1$	199 846	199 861	199 884	199 920	201 691	201 598	−93
$3s4d\ ^3D_2$	200 003	199 857	199 881	199 928	201 666	201 598	−68
$3s4d\ ^3D_3$	200 134	199 855	199 879	199 934	201 634	201 599	−35
$3s4d\ ^1D_2$	202 714	202 640	202 662	202 713	204 464	204 331	−133
$3s4f\ ^1F^o_3$	203 063	202 705	202 716	202 733	204 795	204 828	33
$3p3d\ ^1D^o_2$	203 175	202 977	202 996	203 047	205 357	205 029	−328
$3s5s\ ^3S_1$	204 234	204 288	204 303	204 359	206 118	206 176	58
$3s5s\ ^1S_0$	205 920	205 971	205 988	206 039	207 828	207 874	46
$3s4f\ ^3F^o_2$	207 666	207 551	207 571	207 627	209 597	209 531	−66
$3s4f\ ^3F^o_3$	207 622	207 578	207 597	207 652	209 612	209 559	−53
$3s4f\ ^3F^o_4$	207 574	207 616	207 635	207 687	209 637	209 600	−37
$3s5p\ ^1P^o_1$	212 511	212 566	212 587	212 639	214 504	214 532	28
$3s5p\ ^3P^o_2$	213 130	213 157	213 173	213 213	214 998	214 989	−9
$3s5p\ ^3P^o_1$	213 159	213 142	213 163	213 212	215 002	214 995	−7
$3s5p\ ^3P^o_0$	213 160	213 133	213 157	213 210	215 005	214 995	−10
$3p3d\ ^3P^o_2$	214 375	214 269	214 285	214 319	216 450	216 190	−260
$3p3d\ ^3P^o_1$	214 967	214 376	214 391	214 431	216 613	216 289	−324
$3p3d\ ^3P^o_0$	215 325	214 440	214 453	214 496	216 717	216 350	−367
$3p3d\ ^3D^o_1$	216 019	215 773	215 793	215 839	217 724	217 386	−338
$3p3d\ ^3D^o_2$	216 518	215 881	215 898	215 925	217 743	217 440	−303
$3p3d\ ^3D^o_3$	216 356	215 827	215 845	215 884	217 736	217 489	−247
$3s5f\ ^1F^o_{3\ a}$	224 092	223 605	223 620	223 633	225 644	225 526	−118
$3p4s\ ^3P^o_0$	224 260	224 260	224 273	224 322	226 479	226 400	−79
$3p4s\ ^3P^o_1$	224 376	224 389	224 397	224 445	226 597	226 527	−70
$3p4s\ ^3P^o_2$	224 636	224 676	224 677	224 724	226 884	226 820	−64
$3s5d\ ^3D_1$	225 236	225 165	225 187	225 232	227 105	227 081	−24

Notes. The differences ΔE between the final computations and the observed values are shown in the last column. [(*)]Labeling is changed from NIST-standard to better represent the composition of different levels in a Rydberg series, according to our calculations. As an example are two levels labeled with the same $3s5f\ ^1F$ term but different indices are used to distinguish them. Details are given in the text.
References. [(a)]Kramida et al. (2018).

Table A.1. continued.

Level	VV				CV	E_{obs} [(a)]	ΔE
	$n = 10$	$n = 11$	$n = 12$	$n = 13$			
$3s5d\ ^3D_2$	225 179	225 159	225 181	225 230	227 092	227 084	−8
$3s5d\ ^3D_3$	225 124	225 154	225 177	225 226	227 076	227 089	13
$3s5d\ ^1D_2$	225 833	225 714	225 733	225 773	227 695	227 665	−30
$3p4s\ ^1P^o_1$	226 814	226 801	226 778	226 775	228 788	228 700	−88
$3s6s\ ^3S_1$	227 576	227 630	227 648	227 703	229 556	229 623	67
$3s5f\ ^3F^o_2$	228 134	228 194	228 207	228 265	230 201	230 268	67
$3s5f\ ^3F^o_3$	228 133	228 194	228 206	228 264	230 201	230 269	68
$3s5f\ ^3F^o_4$	228 134	228 195	228 217	228 265	230 201	230 271	70
$3s5g\ ^3G_3$	228 135	228 196	228 219	228 266	230 230	230 301	71
$3s5g\ ^3G_4$	228 159	228 208	228 231	228 288	230 232	230 302	70
$3s5g\ ^1G_4$	228 176	228 211	228 233	228 289	230 233	230 302	69
$3s5g\ ^3G_5$	228 169	228 209	228 232	228 288	230 232	230 302	70
$3s6s\ ^1S_0$	228 303	228 359	228 378	228 433	230 301	230 364	63
$3s6p\ ^3P^o_0$	232 356	232 413	232 437	232 493	234 359	234 415	56
$3s6p\ ^3P^o_1$	232 364	232 423	232 446	232 501	234 365	234 428	63
$3s6p\ ^3P^o_2$	232 382	232 443	232 464	232 518	234 381	234 442	61
$3p3d\ ^1P^o_1$ (*)	233 982	233 003	232982	232 927	234 923	234 388	−535
$3s5f\ ^1F^o_3$ [b]	234 526	233 780	233 783	233 763	235 612	235 414	−198
$3s6p\ ^1P^o_1$ (*)	234 522	234 025	234 033	234 066	235 957	235 951	−6
$3s6d\ ^3D_1$	238 206	238 220	238 231	238 287	240 267	240 262	−5
$3s6d\ ^3D_2$	238 211	238 245	238 256	238 308	240 278	240 284	6
$3s6d\ ^3D_3$	238 224	238 280	238 291	238 338	240 297	240 315	18
$3s6d\ ^1D_2$	238 470	238 484	238 498	238 548	240 537	240 550	13
$3s7s\ ^3S_1$	240 049	240 105	240 124	240 179	242 075	242 145	70
$3s6f\ ^3F^o_2$	240 282	240 327	240 352	240 410	242 336	242 411	75
$3s6f\ ^3F^o_3$	240 277	240 328	240 352	240 409	242 335	242 411	76
$3s6f\ ^3F^o_4$	240 271	240 328	240 352	240 408	242 335	242 412	77
$3s6g\ ^3G_3$	240 301	240 363	240 387	240 440	242 400	242 474	74
$3s6g\ ^3G_4$	240 300	240 364	240 385	240 441	242 403	242 474	71
$3s6g\ ^1G_4$	240 302	240 365	240 388	240 443	242 405	242 474	69
$3s6g\ ^3G_5$	240 301	240 365	240 386	240 443	242 405	242 475	70
$3s7s\ ^1S_0$	240 428	240 487	240 508	240 564	242 466	242 538	72
$3p4p\ ^1P_1$	240 550	240 603	240 625	240 679	242 992	242 885	−107
$3s6f\ ^1F^o_3$	242 239	241 980	241 993	242 017	243 896	243 869	−28
$3p4p\ ^3D_1$	242 550	242 573	242 548	242 602	244 839	244 737	−102
$3s7p\ ^3P^o_0$	242 822	242 881	242 906	242 962	244 862	244 929	67
$3s7p\ ^3P^o_1$	242 827	242 887	242 910	242 966	244 866	244 933	67
$3s7p\ ^3P^o_2$	242 836	242 898	242 920	242 975	244 874	244 943	69
$3p4p\ ^3D_2$	242 665	242 699	242 671	242 723	244 966	244 866	−100
$3p4p\ ^3D_3$	242 864	242 913	242 881	242 930	245 194	245 087	−107
$3s7p\ ^1P^o_1$	243 236	243 291	243 313	243 364	245 250	244 871	−379
$3s7d\ ^1D_2$	245 752	245 805	245 777	245 829	247 946	247 935	−11
$3p4p\ ^3P_0$	245 541	245 588	245 603	245 649	247 965	247 872	−93
$3p4p\ ^3P_1$	245 626	245 675	245 685	245 729	248 040	247 954	−86
$3p4p\ ^3P_2$	245 863	245 922	245 910	245 956	248 239	248 168	−71
$3p4p\ ^3S_1$	246 598	246 609	246 619	246 665	248 952	248 773	−179
$3s7d\ ^3D_1$	247 056	247 068	247 092	247 148	249 067	249 094	27
$3s7d\ ^3D_2$	247 050	247 079	247 102	247 152	249 068	249 104	36
$3s7d\ ^3D_3$	247 045	247 096	247 118	247 160	249 074	249 121	47
$3s7f\ ^3F^o_2$	247 629	247 682	247 707	247 765	249 698	249 774	76
$3s7f\ ^3F^o_3$	247 626	247 683	247 707	247 764	249 697	249 775	78

Table A.1. continued.

Level	VV				CV	E_{obs} [a]	ΔE
	$n = 10$	$n = 11$	$n = 12$	$n = 13$			
3s7f $^3F^o_4$	247 622	247 683	247 707	247 763	249 696	249 775	79
3s7g $^3G_3$	247 648	247 711	247 730	247 786	249 743	249 817	74
3s7g $^3G_4$	247 647	247 711	247 729	247 787	249 746	249 818	72
3s7g $^1G_4$	247 649	247 712	247 732	247 787	249 747	249 818	71
3s7g $^3G_5$	247 648	247 712	247 730	247 788	249 747	249 819	72
3s7f $^1F^o_3$	248 401	248 352	248 371	248 415	250 333	250 366	33

Table A.2. Observed and computed excitation energies for the 29 lowest states in Si III, from present calculations (E_{RCI}) and other theoretical results (E_{theor}).

Level	E_{RCI} [a]	E_{obs} [b]	E_{theor} [c]	E_{theor} [d]	ΔE_{RCI} [a]	ΔE_{theor} [c]	ΔE_{theor} [d]
$3s^2\ ^1S_0$	0	0	0	0	0	0	0
3s3p $^3P^o_0$	52 790	52 725	52 704	51 156	−65	20	1568
3s3p $^3P^o_1$	52 913	52 853	52 835	51 267	−60	18	1586
3s3p $^3P^o_2$	53 164	53 115	53 099	51 491	−49	16	1624
3s3p $^1P^o_1$	83 031	82 884	83 069	84 060	−147	−185	−1176
$3p^2\ ^1D_2$	122 447	122 215	122 487	120 194	−232	−273	2020
$3p^2\ ^3P_0$	129 832	129 708	129 751	128 551	−124	−43	1157
$3p^2\ ^3P_1$	129 953	129 842	129 891	128 664	−111	−50	1177
$3p^2\ ^3P_2$	130 193	130 101	130 153	128 886	−92	−53	1214
3s3d $^3D_3$	143 106	142 944	143 640	142 257	−162	−697	686
3s3d $^3D_2$	143 162	142 946	143 638	142 252	−216	−693	693
3s3d $^3D_1$	143 208	142 948	143 644	142 249	−260	−696	699
3s4s $^3S_1$	153 332	153 377	153 881	151 563	45	−504	1814
$3p^2\ ^1S_0$	153 953	153 444	153 855	155 103	−509	−411	−1659
3s4s $^1S_0$	159 065	159 070	159 604	159 383	5	−535	−314
3s3d $^1D_2$	166 013	165 765	166 490	168 327	−248	−725	−2562
3s4p $^3P^o_0$	175 219	175 230	175 704	174 006	11	−474	1224
3s4p $^3P^o_1$	175 247	175 263	175 743	174 036	16	−480	1227
3s4p $^3P^o_2$	175 312	175 336	175 821	174 102	24	−485	1234
3s4p $^1P^o_1$	176 503	176 487	176 963	175 288	−16	−476	1199
3p3d $^3F^o_2$	199 259	198 923	199 701		−336	−778	
3p3d $^3F^o_3$	199 318	199 026	199 811		−292	−785	
3p3d $^3F^o_4$	199 402	199 164	199 955		−238	−791	
3s4d $^3D_1$	201 691	201 598	202 258		−93	−661	
3s4d $^3D_2$	201 666	201 598	202 263		−68	−665	
3s4d $^3D_3$	201 634	201 599	202 265		−35	−666	
3s4d $^1D_2$	204 464	204 331	205 114		−133	−784	
3s4f $^1F^o_3$	204 795	204 829	205 537		33	−709	
3p3d $^1D^o_2$	205 357	205 029	205 765		−328	−736	

Notes. The theoretical results are compared to values from the NIST-database (E_{obs} [b]). ΔE represents the difference between observed and computed energies. All energies are given in cm^{-1}.
References. [a]Present calculations; [b]Kramida et al. (2018); [c]Froese Fischer et al. (2006); [d]Del Zanna et al. (2015).

Table A.3. Results for Si III: Comparison between computed lifetimes, in length (τ_l) and velocity (τ_v) gauge, from our calculations.

Level	RCI [a]		$\tau_{\text{MCHF-BP}}$ [b]	τ_{MBPT} [c]	τ_{obs} [d]	τ_{obs} [e]
	τ_l	τ_v				
$3s3p\ ^3P^o_1$	7.679E−05	7.822E−05	5.809E−05	1.010E−04		
$3s3p\ ^1P^o_1$	4.024E−10	4.010E−10	4.050E−10	4.290E−10		(4 ± 1)E−10
$3p^2\ ^1D_2$	3.438E−08	3.331E−08	3.273E−08	4.570E−08	(2.60 ± 0.15)E−08	(2.6 ± 0.3)E−08
$3p^2\ ^3P_0$	4.747E−10	4.726E−10	4.779E−10	4.650E−10	(5.0 ± 0.3)E−10[f]	(3.4 ± 1.0)E−10
$3p^2\ ^3P_1$	4.735E−10	4.714E−10	4.764E−10	4.740E−10	(5.0 ± 0.3)E−10[f]	(3.4 ± 1.0)E−10
$3p^2\ ^3P_2$	4.715E−10	4.693E−10	4.741E−10	4.210E−10	(5.0 ± 0.3)E−10[f]	(3.4 ± 1.0)E−10
$3s3d\ ^3D_3$	3.564E−10	3.564E−10	3.524E−10	3.770E−10		
$3s3d\ ^3D_2$	3.540E−10	3.545E−10	3.506E−10	3.740E−10		
$3s3d\ ^3D_1$	3.523E−10	3.531E−10	3.494E−10	3.740E−10		
$3s4s\ ^3S_1$	4.069E−10	4.078E−10	4.068E−10			
$3p^2\ ^1S_0$	4.328E−10	4.306E−10	4.440E−10	4.760E−10	(5.8 ± 0.4)E−10[f]	
$3s4s\ ^1S_0$	1.172E−09	1.178E−09	1.112E−09			
$3s3d\ ^1D_2$	2.185E−10	2.186E−10	2.170E−10	2.320E−10		
$3s4p\ ^3P^o_0$	3.400E−09	3.422E−09	3.409E−09		(3.3 ± 0.3)E−09	(4.1 ± 0.5)E−09
$3s4p\ ^3P^o_1$	3.385E−09	3.403E−09	3.390E−09		(3.6 ± 0.3)E−09	(4.5 ± 0.5)E−09
$3s4p\ ^3P^o_2$	3.367E−09	3.375E−09	3.373E−09			
$3s4p\ ^1P^o_1$	1.972E−09	1.992E−09	1.926E−09			
$3p3d\ ^3F^o_2$	9.971E−07	1.160E−06	1.124E−06	0.023E−06		
$3p3d\ ^3F^o_3$	8.869E−07	1.004E−06	2.210E−06	0.025E−06		
$3p3d\ ^3F^o_4$	9.678E−07	1.272E−06	2.378E−06	0.026E−06		
$3s4d\ ^3D_3$	2.871E−09	2.872E−09	2.818E−09		(3.3 ± 0.3)E−09	(4.0 ± 0.4)E−09
$3s4d\ ^3D_2$	2.837E−09	2.846E−09	2.797E−09		(3.3 ± 0.3)E−09	(4.0 ± 0.4)E−09
$3s4d\ ^3D_1$	2.814E−09	2.829E−09	2.783E−09		(3.3 ± 0.3)E−09	(4.0 ± 0.4)E−09
$3s4d\ ^1D_2$	1.263E−09	1.270E−09	1.294E−09		(1.25 ± 0.15)E−09	(1.9 ± 0.3)E−09
$3s4f\ ^1F^o_3$	6.169E−10	6.185E−10	5.979E−10			
$3p3d\ ^1D^o_2$	4.277E−10	4.273E−10	4.263E−10	3.800E−10		
$3s5s\ ^3S_1$	7.438E−10	7.467E−10				
$3s5s\ ^1S_0$	1.111E−09	1.114E−09				
$3s4f\ ^3F^o_2$	4.795E−10	4.788E−10			(5.1 ± 0.3)E−10[f]	(12 ± 1)E−10
$3s4f\ ^3F^o_3$	4.793E−10	4.786E−10			(5.1 ± 0.3)E−10[f]	(12 ± 1)E−10
$3s4f\ ^3F^o_4$	4.790E−10	4.780E−10			(5.1 ± 0.3)E−10[f]	(12 ± 1)E−10
$3s5p\ ^1P^o_1$	1.279E−09	1.288E−09				
$3s5p\ ^3P^o_2$	2.270E−09	2.276E−09				
$3s5p\ ^3P^o_1$	2.875E−09	2.889E−09				
$3s5p\ ^3P^o_0$	3.253E−09	3.273E−09				
$3p3d\ ^3P^o_2$	3.216E−10	3.225E−10				
$3p3d\ ^3P^o_1$	3.096E−10	3.110E−10				
$3p3d\ ^3P^o_0$	3.056E−10	3.076E−10				
$3p3d\ ^3D^o_1$	2.016E−10	2.025E−10				(3.6 ± 0.4)E−10
$3p3d\ ^3D^o_3$	2.020E−10	2.023E−10				(3.6 ± 0.4)E−10
$3p3d\ ^3D^o_2$	2.023E−10	2.028E−10				(3.6 ± 0.4)E−10
$3s5f\ ^1F^o_3$ *a*	4.807E−10	4.824E−10				(10 ± 5)E−10
$3p4s\ ^3P^o_0$	4.548E−10	4.538E−10				
$3p4s\ ^3P^o_1$	4.520E−10	4.511E−10				
$3p4s\ ^3P^o_2$	4.474E−10	4.468E−10				
$3s5d\ ^3D_3$	8.682E−09	8.748E−09				
$3s5d\ ^3D_2$	8.646E−09	8.735E−09				
$3s5d\ ^3D_1$	8.617E−09	8.734E−09				
$3s5d\ ^1D_2$	5.794E−09	5.833E−09				
$3p4s\ ^1P^o_1$	4.245E−10	4.246E−10				
$3s6s\ ^3S_1$	1.285E−09	1.291E−09				

Notes. The present values from the RCI calculations are compared to the predicted lifetimes from MCHF-BP [b] ($\tau_{\text{MCHF-BP}}$) and MBPT [c] (τ_{MBPT}) models, as well as experimental results τ_{obs} [d],[e], with stated uncertainties. All values are given in seconds.

References. [a]Present calculations; [b]Froese Fischer et al. (2006); [c]Safronova et al. (2000); [d]Bashkin et al. (1980); [e]Berry et al. (1971); [f]Livingston et al. (1976b).

Table A.3. continued.

Level	RCI [a]		$\tau_{\text{MCHF-BP}}$ [b]	τ_{MBPT} [c]	τ_{obs} [d]	τ_{obs} [e]
	τ_{l}	τ_{v}				
3s5f $^3F^o_3$	9.537E−10	9.544E−10				(14 ± 2)E−10
3s5f $^3F^o_2$	9.555E−10	9.566E−10				(14 ± 2)E−10
3s5f $^3F^o_4$	9.511E−10	9.517E−10				(14 ± 2)E−10
3s5g $^3G_3$	2.775E−09	2.772E−09				(4.3 ± 0.5)E−09
3s5g $^3G_4$	2.776E−09	2.773E−09				(4.3 ± 0.5)E−09
3s5g $^3G_5$	2.775E−09	2.773E−09				(4.3 ± 0.5)E−09
3s5g $^1G_4$	2.779E−09	2.774E−09				
3s6s $^1S_0$	1.810E−09	1.815E−09				
3s6p $^3P^o_0$	9.157E−09	9.335E−09				
3s6p $^3P^o_1$	8.981E−09	9.117E−09				
3s6p $^3P^o_2$	9.032E−09	9.105E−09				
3p3d $^1P^o_1$	2.809E−10	2.843E−10				
3s5f $^1F^o_3$ [b]	3.995E−10	4.003E−10				
3s6p $^1P^o_1$	1.129E−09	1.136E−09				
3s6d $^3D_1$	5.243E−09	5.354E−09				
3s6d $^3D_2$	5.548E−09	5.645E−09				
3s6d $^3D_3$	5.953E−09	6.035E−09				
3s6d $^1D_2$	1.081E−08	1.095E−08				
3s7s $^3S_1$	2.009E−09	2.021E−09				
3s6f $^3F^o_4$	1.676E−09	1.679E−09				
3s6f $^3F^o_3$	1.684E−09	1.687E−09				
3s6f $^3F^o_2$	1.690E−09	1.695E−09				
3s6g $^3G_3$	4.764E−09	4.748E−09				
3s6g $^3G_4$	4.782E−09	4.763E−09				
3s6g $^1G_4$	4.802E−09	4.793E−09				
3s6g $^3G_5$	4.759E−09	4.754E−09				
3s7s $^1S_0$	2.849E−09	2.859E−09				
3p4p $^1P_1$	6.436E−10	6.446E−10				
3s6f $^1F^o_3$	8.651E−10	8.659E−10				
3p4p $^3D_1$	7.732E−10	7.724E−10				
3s7p $^3P^o_0$	1.524E−08	1.561E−08				
3s7p $^3P^o_1$	1.521E−08	1.551E−08				
3s7p $^3P^o_2$	1.518E−08	1.535E−08				
3p4p $^3D_2$	7.715E−10	7.714E−10				
3p4p $^3D_3$	7.665E−10	7.664E−10				
3s7p $^1P^o_1$	7.755E−09	7.978E−09				
3s7d $^1D_2$	3.670E−09	3.710E−09				
3p4p $^3P_0$	7.308E−10	7.301E−10				
3p4p $^3P_1$	7.334E−10	7.326E−10				
3p4p $^3P_2$	7.504E−10	7.493E−10				
3p4p $^3S_1$	9.027E−10	9.046E−10				
3s7d $^3D_1$	6.279E−09	6.118E−09				
3s7d $^3D_2$	5.964E−09	5.850E−09				
3s7d $^3D_3$	5.550E−09	5.492E−09				
3s7f $^3F^o_4$	2.689E−09	2.697E−09				
3s7f $^3F^o_3$	2.708E−09	2.718E−09				
3s7f $^3F^o_2$	2.722E−09	2.736E−09				
3s7g $^3G_3$	7.614E−09	7.543E−09				
3s7g $^3G_4$	7.632E−09	7.616E−09				
3s7g $^1G_4$	7.804E−09	7.727E−09				
3s7g $^3G_5$	7.610E−09	7.609E−09				
3s7f $^1F^o_3$	1.713E−09	1.723E−09				

Table A.4. Computed excitation energies in cm^{-1} for the 45 lowest states in Si IV, as a function of the increasing active set of orbitals, accounting for CV correlation, where n indicates the maximum principle quantum number of the orbitals included in the active set, as well as CC correlation.

	CV							
Level	$n = 10$	$n = 11$	$n = 12$	CC	E_{obs} [(a)]	E_{theor} [(b)]	ΔE_{CC}	ΔE_{theor} [(b)]
$3s\ ^2S_{1/2}$	0	0	0	0	0	0	0	0
$3p\ ^2P^o_{1/2}$	71 407	71 353	71 351	71 211	71 288	71 159	77	128
$3p\ ^2P^o_{3/2}$	71 870	71 813	71 812	71 667	71 749	71 667	82	81
$3d\ ^2D_{5/2}$	160 585	161 039	161 209	160 208	160 374	160 287	166	87
$3d\ ^2D_{3/2}$	160 587	161 041	161 210	160 210	160 376	160 281	166	94
$4s\ ^2S_{1/2}$	194 179	194 571	194 709	193 778	193 979	193 787	201	192
$4p\ ^2P^o_{1/2}$	218 498	218 859	218 986	218 048	218 267	218 051	219	216
$4p\ ^2P^o_{3/2}$	218 661	219 020	219 147	218 208	218 429	218 234	221	194
$4d\ ^2D_{5/2}$	250 200	250 743	250 933	249 767	250 008	249 827	241	181
$4d\ ^2D_{3/2}$	250 200	250 743	250 933	249 768	250 008	249 821	240	187
$4f\ ^2F^o_{5/2}$	254 313	254 927	255 134	253 847	254 127	253 876	280	251
$4f\ ^2F^o_{7/2}$	254 315	254 929	255 136	253 848	254 129	253 880	281	249
$5s\ ^2S_{1/2}$	265 617	266 135	266 312	265 166	265 418	265 216	252	202
$5p\ ^2P^o_{1/2}$	276 718	277 218	277 387	276 244	276 504	276 281	260	223
$5p\ ^2P^o_{3/2}$	276 794	277 293	277 462	276 319	276 579	276 365	260	214
$5d\ ^2D_{5/2}$	291 680	292 265	292 464	291 232	291 498	291 292	266	206
$5d\ ^2D_{3/2}$	291 680	292 265	292 464	291 232	291 498	291 290	266	208
$5f\ ^2F^o_{5/2}$	293 898	294 519	294 727	293 431	293 719	293 475	288	244
$5f\ ^2F^o_{7/2}$	293 899	294 520	294 728	293 432	293 719	293 477	287	242
$5g\ ^2G_{7/2}$	294 007	294 638	294 847	293 549	293 838		289	
$5g\ ^2G_{9/2}$	294 008	294 638	294 848	293 550	293 838		288	
$6s\ ^2S_{1/2}$	299 865	300 436	300 628	299 406	299 677	299 451	271	226
$6p\ ^2P^o_{1/2}$	305 839	306 398	306 585	305 365	305 641	305 405	276	236
$6p\ ^2P^o_{3/2}$	305 881	306 439	306 626	305 406	305 682	305 450	276	232
$6d\ ^2D_{3/2}$	314 092	314 698	314 901	313 638	313 915	313 688	277	227
$6d\ ^2D_{5/2}$	314 092	314 698	314 901	313 638	313 915	313 690	277	225
$6f\ ^2F^o_{5/2}$	315 404	316 031	316 239	314 939	315 230	314 983	291	248
$6f\ ^2F^o_{7/2}$	315 404	316 031	316 240	314 940	315 230	314 983	290	247
$6g\ ^2G_{7/2}$	315 475	316 106	316 315	315 016	315 305		289	
$6g\ ^2G_{9/2}$	315 475	316 106	316 316	315 016	315 305		289	
$6h\ ^2H^o_{9/2}$	315 482	316 118	316 327	315 023	315 317		294	
$6h\ ^2H^o_{11/2}$	315 482	316 118	316 328	315 023	315 317		294	
$7s\ ^2S_{1/2}$	318 924	319 520	319 719	318 463	318 743	318 505	280	238
$7p\ ^2P^o_{1/2}$	322 500	323 089	323 285	322 029	322 313	322 069	284	244
$7p\ ^2P^o_{3/2}$	322 525	323 114	323 309	322 054	322 338	322 097	284	241
$7d\ ^2D_{3/2}$	327 536	328 153	328 358	327 080	327 362	327 125	282	237
$7d\ ^2D_{5/2}$	327 536	328 153	328 358	327 080	327 362	327 125	282	237
$7f\ ^2F^o_{5/2}$	328 370	329 001	329 210	327 908	328 200	327 950	292	251
$7f\ ^2F^o_{7/2}$	328 371	329 001	329 210	327 908	328 200	327 950	292	250
$7g\ ^2G_{7/2}$	328 418	329 050	329 260	327 959	328 250		291	
$7g\ ^2G_{9/2}$	328 419	329 051	329 260	327 959	328 250		291	
$7h\ ^2H^o_{9/2}$	328 423	329 059	329 269	327 963	328 257		294	
$7h\ ^2H^o_{11/2}$	328 423	329 059	329 269	327 964	328 257		293	
$7i\ ^2I_{11/2}$	328 424	329 060	329 270	327 965	328 261		296	
$7i\ ^2I_{13/2}$	328 425	329 061	329 270	327 965	328 261		296	

Notes. Observed and computed excitation energies for the Si IV from the NIST-database (E_{obs} [(a)]) and the other theoretical study (E_{theor} [(b)]) are also given. In the last two columns, the difference ΔE between observed and computed energies is compared for the present and previous studies.
References. [(a)]Kramida et al. (2018); [(b)]Froese Fischer et al. (2006).

Table A.5. Results for Si IV: Comparison between computed lifetimes, in length (τ_l) and velocity (τ_v) gauge, from our calculations.

Level	RCI [a]		τ_{theor} [b]	τ_{theor} [c]	τ_{obs} [d]	τ_{obs} [e]
	τ_l	τ_v				
$3p\ ^2P^o_{1/2}$	1.162E−09	1.159E−09	1.167E−09	1.102E−09		(1.2 ± 0.4)E−09
$3p\ ^2P^o_{3/2}$	1.139E−09	1.138E−09	1.141E−09	1.081E−09		(1.2 ± 0.4)E−09
$3d\ ^2D_{3/2}$	3.923E−10	3.906E−10	3.916E−10	3.790E−10		(4.6 ± 0.5)E−10
$3d\ ^2D_{5/2}$	3.964E−10	3.949E−10	3.962E−10	3.840E−10		(4.6 ± 0.5)E−10
$4s\ ^2S_{1/2}$	2.819E−10	2.827E−10	2.821E−10	2.930E−10		
$4p\ ^2P^o_{1/2}$	9.156E−10	9.150E−10	9.111E−10	9.970E−10		(7.5 ± 0.3)E−10
$4p\ ^2P^o_{3/2}$	9.232E−10	9.221E−10	9.199E−10	9.900E−10		(7.5 ± 0.3)E−10
$4d\ ^2D_{3/2}$	1.808E−09	1.812E−09	1.806E−09	1.824E−09	(2.0 ± 0.2)E−09	(2.1 ± 0.2)E−09
$4d\ ^2D_{5/2}$	1.811E−09	1.816E−09	1.810E−09	1.846E−09	(2.0 ± 0.2)E−09	(2.1 ± 0.2)E−09
$4f\ ^2F^o_{5/2}$	2.638E−10	2.638E−10	2.639E−10	2.620E−10		(4.8 ± 0.4)E−10
$4f\ ^2F^o_{7/2}$	2.638E−10	2.638E−10	2.639E−10	2.620E−10		(4.8 ± 0.4)E−10
$5s\ ^2S_{1/2}$	4.348E−10	4.356E−10	4.322E−10	4.460E−10		
$5p\ ^2P^o_{1/2}$	1.288E−09	1.283E−09	1.269E−09	1.382E−09	(2.1 ± 0.3)E−09	(2.2 ± 0.2)E−09
$5p\ ^2P^o_{3/2}$	1.299E−09	1.293E−09	1.283E−09	1.375E−09	(2.1 ± 0.3)E−09	(2.2 ± 0.2)E−09
$5d\ ^2D_{3/2}$	3.090E−09	3.100E−09	3.058E−09	3.231E−09		
$5d\ ^2D_{5/2}$	3.068E−09	3.078E−09	3.036E−09	3.256E−09		
$5f\ ^2F^o_{5/2}$	4.940E−10	4.934E−10	4.926E−10			
$5f\ ^2F^o_{7/2}$	4.940E−10	4.935E−10	4.927E−10	4.820E−10		
$5g\ ^2G_{7/2}$	9.147E−10	9.154E−10		9.240E−10	(12 ± 2)E−10	(26 ± 3)E−10
$5g\ ^2G_{9/2}$	9.147E−10	9.154E−10		9.240E−10	(12 ± 2)E−10	(26 ± 3)E−10
$6s\ ^2S_{1/2}$	7.062E−10	7.058E−10	6.952E−10	7.160E−10		
$6p\ ^2P^o_{1/2}$	1.957E−09	1.937E−09	1.901E−09	2.063E−09		
$6p\ ^2P^o_{3/2}$	1.975E−09	1.952E−09	1.921E−09	2.056E−09		
$6d\ ^2D_{3/2}$	4.529E−09	4.488E−09	4.376E−09	4.685E−09		
$6d\ ^2D_{5/2}$	4.482E−09	4.445E−09	4.332E−09	4.712E−09		
$6f\ ^2F^o_{5/2}$	8.336E−10	8.289E−10	8.274E−10			
$6f\ ^2F^o_{7/2}$	8.336E−10	8.290E−10	8.274E−10	8.070E−10		
$6g\ ^2G_{7/2}$	1.568E−09	1.569E−09				
$6g\ ^2G_{9/2}$	1.568E−09	1.569E−09		1.569E−09		
$6h\ ^2H^o_{9/2}$	2.373E−09	2.374E−09				(5.2 ± 0.5)E−09
$6h\ ^2H^o_{11/2}$	2.373E−09	2.374E−09		2.376E−09		(5.2 ± 0.5)E−09
$7s\ ^2S_{1/2}$	1.116E−09	1.110E−09	1.077E−09	1.110E−09		
$7p\ ^2P^o_{1/2}$	3.010E−09	2.911E−09	2.808E−09	3.040E−09		
$7p\ ^2P^o_{3/2}$	3.035E−09	2.934E−09	2.837E−09	3.034E−09		
$7d\ ^2D_{3/2}$	6.832E−09	6.366E−09	6.073E−09	6.542E−09		
$7d\ ^2D_{5/2}$	6.732E−09	6.300E−09	6.007E−09	6.553E−09		
$7f\ ^2F^o_{5/2}$	1.325E−09	1.294E−09	1.289E−09			
$7f\ ^2F^o_{7/2}$	1.325E−09	1.294E−09	1.289E−09	1.261E−09		
$7g\ ^2G_{7/2}$	2.473E−09	2.469E−09				
$7g\ ^2G_{9/2}$	2.473E−09	2.470E−09		2.454E−09		
$7h\ ^2H^o_{9/2}$	3.751E−09	3.752E−09				
$7h\ ^2H^o_{11/2}$	3.751E−09	3.753E−09		3.750E−09		
$7i\ ^2I_{11/2}$	5.270E−09	5.272E−09				
$7i\ ^2I_{13/2}$	5.270E−09	5.272E−09		5.267E−09		

Notes. The present values from the RCI calculations are compared to the predicted lifetimes from other calculations [b],[c] (τ_{theor}), as well as experimental results τ_{obs} [d],[e], with stated uncertainties. All values are given in seconds.
References. [a]Present calculations; [b]Froese Fischer et al. (2006); [c]Siems et al. (2001); [d]Bashkin et al. (1980); [e]Berry et al. (1971).